A Discrete Element Method based-approach for arched masonry structures under blast loads

Filippo Masi, Ioannis Stefanou, Victor Maffi-Berthier, Paolo Vannucci

A Discrete Element Method based-approach for arched masonry structures under blast loads

Filippo Masi[a,b,d,*], Ioannis Stefanou[a,d], Victor Maffi-Berthier[b], Paolo Vannucci[c]

[a]Laboratoire Navier, UMR 8205, École des Ponts, IFSTTAR, CNRS, UPE,
6-8 avenue Blaise Pascal, F-77455, Champs-sur-Marne, France.

[b]Ingérop Conseil et Ingénierie,
18 rue des Deux Gares, F-92500, Rueil-Malmaison, France.

[c]LMV, UMR 8100, Université de Versailles et Saint-Quentin,
55 avenue de Paris, F-78035, Versailles, France.

[d]Present address:
Research Institute in Civil and Mechanical Engineering (GeM), École Centrale de Nantes,
1 rue de la Noë, F-44321, Nantes, France.

Abstract

Masonry structures are often characterized by complex, non-planar geometries. This is also the case for historical and monumental structures. Here we investigate the dynamic behaviour of non-standard, curvilinear masonry geometries, such as vaults, subjected to blast loading.

We use the Discrete Element Method (DEM) for modelling the dynamic structural response to explosions. The approach allows considering the detailed mechanical and geometrical characteristics of masonry, as well as the inherent coupling between the in- and out-of-plane motion.

The proposed modelling approach is validated with existing experimental tests in the case of planar masonry geometries, walls, subjected to far-field explosions. The DEM model is found to satisfactorily capture the dynamic response of the system and the form of failure within the body of the masonry structure.

Then the response of an emblematic curved masonry structure subjected to blast loading is investigated. The influence of various micro-mechanical parameters, such as the dilatancy angle, the tensile strength and the cohesion of the masonry joints on the overall dynamic structural response of the system is explored. The effect of the size of the building blocks is also studied.

Masonry joints with zero dilatancy lead to increased out-of-plane deformations and reduced membrane ones, with respect to associative case. Cohesion and tensile strength are found to have negligible influence on the structural response. The size of the building blocks shapes the overall strength of the system.

Finally, the performance of a discrete model with infinitely rigid blocks is explored and evaluated through detailed comparisons of the parametric numerical tests using deformable blocks. The rigid blocks model predictions, for the loading conditions and geometries here investigated, are found to be affected by the rotational locking effect.

Keywords: Masonry; Discrete Element Method (DEM); Blast loads; Dilatancy; Scale effect.

1. Introduction

The analysis of masonry structures and their behaviour attracts significant scientific research, mostly due to the fact that the vast majority of historical buildings and a considerable part of modern constructions are indeed made of masonry. Until now, attention was mainly focused on the mechanical behaviour of masonry under quasi-static and seismic loads using experimental, numerical, and/or theoretical means, see e.g. [47, 27, 45, 44, 16, 15, 6, 5, 25].

The motivation of this work lies in the present international context. There is currently a need for the scientific community and institutions to better assess the threat of explosions meant to destroy civil engineering assets. Emblematic monumental brick and stone structures are often primary targets. In the existing, public (non-confidential) literature, neither experimental nor numerical investigations of the response to explosions of typical structural elements of such architectural assets exist. Here we refer to arches, vaults, domes, etc. To this purpose, we use a Discrete Element Method (DEM) approach to

*Corresponding author.
Email addresses: filippo.masi@ec-nantes.fr (Filippo Masi), ioannis.stefanou@ec-nantes.fr (Ioannis Stefanou), victor.maffi-berthier@ingerop.com (Victor Maffi-Berthier), paolo.vannucci@uvsq.fr (Paolo Vannucci)

analyse the blast loading response of a typical arched masonry structure: a barrel vault. This geometry is taken as paradigm–due to the interplay between membrane (in-plane) and bending (out-of-plane) modes of deformation and failure–in order to better understand the dynamic behaviour of such kind of assets and to identify the dominant parameters that influence their response.

The analysis of the blast loads effects on masonry structures received increased attention in the last two decades, although limited to simple flat walls. We record, for instance, the work of Varma et al. [52] who performed tests on several masonry panels of different thickness subjected to near- and far-field explosions. Gabrielsen et al. [13] experimentally investigated the response to blast loading of full-scale un-reinforced masonry walls with and without development of arching actions (which stem in the out-of-plane response of a wall butted against rigid supports). The strength enhancement of one-way arching masonry walls comes from arising of (beneficial) compressive membrane stresses in the out-of-plane response. Dennis et al. [8] conducted experiments on 1/4-scale reinforced masonry walls under blast events. Abou-Zeid et al. [1] studied the response of arching walls made of hollow concrete bricks under several explosive weights, in a far-field scenario. Gagnet et al. [14] performed full-scale explosion tests on masonry walls to investigate the influence of boundary conditions in the development of compressive arching actions. Keys and Clubley [20] investigated masonry debris distribution and failure patterns of masonry walls when subjected to long duration blast loading. Propagation of cracks was found to occur almost exclusively along the bed joints and damage within the body of individual bricks was negligible. Li et al. [26] investigated through experimental and numerical studies the response of un-reinforced clay brick masonry walls subjected to vented gas explosions. More recently, Michaloudis and Gebbeken [34] analysed the response of unreinforced masonry walls constrained to rigid supports and subjected to far-field and contact explosions. The approach was both experimental and numerical. In the case of far-field explosions, global collapse was induced by the failure at the interfaces between blocks and damage of bricks was negligible. To the authors' knowledge, this is the most recent and well-documented experimental work and for this reason will be used as reference for comparison and validation of the proposed model.
It is worth emphasizing that a similar research activity is not reported for non-standard curved masonry structures, despite the fact that non-planar shapes are common in many monumental structures of high risk (e.g. Gothic cathedrals [51, 49, 50]) and more modern ones ([57, 9]).

As far it concerns numerical modelling of masonry under fast-dynamic excitations, macro-modelling/continuum approaches dominate in the available literature. Among others, we record Wang et al. [54] who developed a predictive method for fragment size and ejection distance of masonry wall under blast loads using a homogenized approach. Wei and Stewart [56] tested the response of masonry walls of different thickness and supporting conditions under far-field blasts with a meso-scale numerical approach. Macorini and Izzuddin [30] performed numerical tests of unreinforced masonry walls through a meso-macro partitioned numerical model. Hashemi Rafsanjani et al. [39] proposed a strain rate dependent anisotropic continuum model for masonry subjected to high rate loading and investigated the influence of tensile strength and wall thickness. Parisi et al. [35] investigated through a finite element macro-model the out-of-plane blast performance of tuff stone masonry walls. Silva et al. [29] developed a homogenized approach accounting for high strain rate effects to analyse masonry panels subjected to impact and blast loads.

The main goal of this paper is to extend the existing knowledge, from both experimental and numerical evidences, of the behaviour of planar masonry structures subjected to explosions to the aforementioned non-standard, arched ones. We consider herein ancient and modern masonry with bricks connected by (mortared or dry) joints, for which the strength of the latter is smaller than the strength of former (≈ 1 order of magnitude). This results in enhanced weakness and structural vulnerability at the interfaces [47, 45, 15].
A Discrete Element (DE) model is adopted for accessing the salient features of the system keeping at minimum the modelling assumptions. The methodology is presented in Section 2. Blast loads are computed using a dynamic library which accounts for the effect of surface rotation of building blocks as well as the evolution in time of their relative distance with respect to the impinging blast wave, as discussed in Section 3. In Section 4, the model is validated with the available experimental results in [34], and, in Section 5, numerical tests are performed to investigate the influence of the micro-mechanical and geometric parameters on the response of a curvilinear masonry structure to surface blasts. Finally, we explore the appropriateness of a rigid blocks assumption in the DE simulations in Section 6.

2. Discrete Element Model and modelling assumptions

Herein we rely on the Discrete Element Method to investigate the behaviour of masonry structures. The approach allows to directly model several micro-mechanical parameters, such as the geometry of the building blocks and the constitutive behaviour of the interfaces and of the blocks. A discrete approach further allows to simulate the progressive failure of masonry and capture with fidelity the post-peak, softening, dynamic behaviour of a masonry structure with bricks undergoing large displacements and rotations [15, 5, 25, 32].
DEM simulations are carried out using 3DEC software [18]. A central finite differences scheme is used for integrating in time the equations of motion of each block. A

soft-contact algorithm is used to model the interactions between neighbouring blocks through interfaces/joints, which are discretized into triangular sub-contact zones [18].

Herein we consider masonry structures whose interfaces have reduced strength compared to that of the bricks. This is usually the case for ancient and modern masonry (cf. [47, 45, 15]). Under such circumstances, damage usually occurs at the joints. At variance of other approaches, this allows us to avoid modelling the strain rate effects in the numerical analyses, at the level of both masonry joints and blocks. Indeed, extensive research showed increased resistance of brittle materials, at increasing loading rates, mainly due to the finite growth rate of micro-cracks [11, 12] and the viscosity of the material [55]. In particular, the dynamic increase factor for tensile/compressive strength for geo-materials (such as mortar, tuff, concrete, marble, cement paste, etc.) usually varies between 1 and ≈ 7 depending on the developed strain rates, see e.g. [41, 7]. Such phenomenon may affect the dynamic response of both bricks and joints within the masonry. Nevertheless, for all applications here investigated the increase in strength at high rates can be neglected for the masonry joints (safety side considerations), as it is shown in Section 4 where the numerical predictions (based on mechanical parameters that are determined by a static characterisation of materials [27, 46, 58, 38]) agree with the experimental evidence.

We model the masonry bricks as deformable blocks interacting through zero thickness contact interfaces, and subdivided into finite-difference meshes of tetrahedral elements. Accounting for blocks deformability increases considerably the calculation time, compared to simulations using infinitely rigid ones. This is why the pertinence of the simplifying assumption of rigid blocks is discussed in Section 6.

Finally, for all simulations involving blast loading, no damping, neither at the material level nor artificially in the analyses, is considered to avoid any attenuation of high-frequency modes of response.

2.1. Constitutive behaviour of masonry joints

2.1.1. Elastic behaviour

The elastic behaviour of the interfaces is defined through the following stress-displacement relationship [18]:

$$\begin{pmatrix} t_n \\ t_t \end{pmatrix} = \begin{pmatrix} k_n & 0 \\ 0 & k_t \end{pmatrix} \begin{pmatrix} u_n \\ u_t \end{pmatrix}, \qquad \text{or} \qquad \boldsymbol{t} = \boldsymbol{k^{el}}\, \boldsymbol{u}, \tag{1}$$

where $\boldsymbol{t}$ and $\boldsymbol{u}$ are the vectors collecting the normal, t_n, and tangential, t_t, forces per joint's unit area and the joint normal, u_n, and tangential, u_t, displacement, respectively. The elastic stiffness matrix $\boldsymbol{k^{el}}$ collects the normal and tangential stiffness: k_n and k_t, respectively.
Normal and tangential stiffness are computed from the properties of the masonry components and the soft-contact assumption. For a deformable block model, the elastic parameters read:

$$k_n = \frac{E_m}{h_m} \qquad \text{and} \qquad k_t = \frac{G_m}{h_m}, \tag{2}$$

where E_m and G_m represent the Young's and shear moduli of mortar, respectively, and h_m is the thickness of the masonry joints (for more, we refer to [32]). The lumping estimation (2), usually adopted in the existing literature (cf. [15, 31]), is based on in-plane loading of planar structures [42]. Expression (2) is considered for both head and bed joints.

2.1.2. Plastic and softening behaviour

In the absence of more detailed experimental data regarding the behaviour and the resistance of masonry joints, the Coulomb criterion seems to be a reasonable choice. Several experimental observations (e.g. [47, 28, 53]) justify its use up to moderate compression.

The maximum shear (tangential) force per joint's unit area t_t is limited by the Coulomb failure surface:

$$f_1 = t_t - c - t_n \tan\varphi \leq 0, \tag{3}$$

where c is the cohesion of the interface, φ the friction angle. Compression is here considered negative. In shear/tensional regime a tension cut-off is often used as shown in Figure 1. In other words, the maximum normal force per joint's unit area t_n is limited by the tensile strength according to:

$$f_2 = t_n - f_t \leq 0, \tag{4}$$

where f_t is the tensile strength of the interface. The normal force F_n and shear force F_t vectors at the sub-contacts (i.e., discretized zones of the interfaces) are

$$F_t = A_j t_t \quad \text{and} \quad F_n = A_j t_n, \tag{5}$$

where A_j is the sub-contact area, which is updated at each time increment (for more, we refer to [18]).
We stress that the strength of the masonry joints is retrieved from static characterisation of the material. The dynamic increase due to strain rate effects is not taken into account to be on the safety side, as we consider masonry structures with weak joints. The built-in constitutive law presently implemented in 3DEC does not account for joint compressive failure. Although solutions to overcome such issue have been implemented in the existing literature (see e.g. [31]), as it follows, an infinite compressive strength of the masonry joints is assumed. This hypothesis is a posteriori verified by monitoring the compressive stresses in the numerical computations.

The two inequalities (3, 4) define the elastic domain of masonry joints. These surfaces can evolve and contract under combined shear and normal plastic deformation in order to take into account various micro-mechanisms related to progressive softening of the joints. As observed in

experimental results on interfaces, a softening behaviour, as depicted in Figure 1, is observed. Accordingly, maximum tensile strength, cohesion, friction angle, and dilatancy, ψ, can evolve from their initial values c; f_t; φ; ψ to some smaller residual values c_{res}; $f_{t_{res}}$; φ_{res}; ψ_{res}. All these values can be determined by experimental tests on interfaces. Regarding the plastic flow rule, this is given by the following potentials:

$$g_1 = t_t - t_n \tan\psi, \tag{6}$$

$$g_2 = t_n. \tag{7}$$

If $\psi = \varphi$ we say that the plastic flow rule is associative (normality condition), otherwise ($\psi < \varphi$) the material obeys a non-associative plastic flow rule. In both cases, the following general relation between the rate of change of forces and the rate of change of total displacements stands:

$$\dot{\boldsymbol{t}} = \boldsymbol{k}^{\boldsymbol{pl}} \dot{\boldsymbol{u}}, \tag{8}$$

with $\boldsymbol{k}^{\boldsymbol{pl}}$ the plasticity matrix,

$$\boldsymbol{k}^{\boldsymbol{pl}} = \frac{k_n}{\kappa + \tan\varphi \tan\psi} \begin{pmatrix} \tan\psi & 1 \\ \tan\varphi \tan\psi & \tan\varphi \end{pmatrix},$$

where $\kappa = k_n/k_s$, and $\dot{\boldsymbol{t}}$ and $\dot{\boldsymbol{u}}$ represent the rate of change of the forces and of the total displacement vectors, $\boldsymbol{t}$ and $\boldsymbol{u}$, respectively.

2.2. Constitutive behaviour of masonry blocks

Blocks are assumed to follow an elastic, isotropic material behaviour. In the DE model, joints have zero thickness, which is not the case in real masonry. For this purpose, the elastic parameters of the blocks have to be modified in order to account for the finite thickness of the joints [32]. Namely, the Young's and shear moduli of the discrete elements become:

$$E_b^* = E_b \left(1 + \frac{h_m}{h_b}\right) \qquad \text{and} \qquad G_b^* = G_b \left(1 + \frac{h_m}{h_b}\right), \tag{9}$$

with E_b and G_m being the Young's and shear moduli of the masonry bricks, respectively; h_b is the height of the masonry bricks; h_m is the mortar joints' thickness. Notice that the difference between the elastic parameters, E_b and G_m, and the corrected ones, E_b^* and G_m^*, is very small ($\approx 5 \div 10$ %) and in general negligible, for typical masonries.

We further assume infinite tensile and compressive strength for the blocks. This may be a strong assumption in the case of near-field explosions and especially in contact detonations, see e.g. [34]. Nevertheless, experimental evidence shows that damage is generally negligible within the body of masonry bricks in moderate to far-field explosions. In these conditions, the collapse of the masonry structure is governed by failure at the interfaces [1, 20, 34].
In each computation, strain rates inside the bricks are monitored to verify that the related dynamic strength of the material is such that failure does not occur. This was true for all simulations presented herein.

3. Blast loads

Explosion produces a blast wave of high-pressure accompanying high-temperature and supersonic expansion of gases. The abrupt increase of the pressure carried by a blast wave can produce severe structural damage. When the primary shock meets a target, it generates on it the so-called reflected overpressure, P_r, which is the difference between the pressure determined by the explosion increased by the reflection at target's surface and the ambient one, P_o. Figure 2 shows the schematic time variation of P_r, which is determined by the arrival time of the shock wave, t_A, the overpressure peak, P_{ro}, the positive phase duration, t_o, negative phase duration, t_{o-}, and the underpressure peak, P_{ro-}. These parameters are functions of the distance R and the explosive weight (conventionally expressed in TNT equivalent).

The simulation of a blast can be conducted by using different approaches [40, 22]. Herein we refer to empirical models based on experimental results available in the existing literature.

3.1. Blast model

We model blast actions following the work of Hyde [17] with the empirical model ConWep, which relies on the best-fit interpolations of the experimental results from Kingery and Bulmash [21]. The interpolations allow to determine the blast parameters and pressure loading from the knowledge of the trinitrotoluene (TNT) equivalent explosive weight, W, and the Hopkinson-Cranz scaled distance, $Z = R/\sqrt[3]{W}$. The time evolution of the reflected pressure is modelled with the well established modified Friedlander equation,

$$P_r(t) = P_{ro}\left(1 - \frac{t}{t_o}\right)\exp\left(-d\frac{t}{t_o}\right), \tag{10}$$

where d is the exponential decay coefficient. The impulse associated to the positive, i_{r+}, and the negative phase, i_{r-}, reads:

$$i_{r+} = \int_0^{t_o} P_{r+}\, dt = \left[e^{-d} + d - 1\right]\frac{P_{ro}\, t_o}{d^2}, \tag{11}$$

$$i_{r-} = \int_{t_o}^{\infty} P_r\, dt = -\frac{P_{ro}\, t_o}{d^2} e^{-d}, \tag{12}$$

respectively. Equation 11 allows to determine the exponential decay coefficient, d, by equating it with the best-fit interpolation of i_{r+} from experiments [21].

ConWep model is able to accurately predict the blast loads in the frame of moderate to far-field scenarios, i.e., for scaled distances $Z \geq 0.4$ m/kg$^{1/3}$ (see [3, 19, 43]). In the near-field, $Z < 0.1$ m/kg$^{1/3}$, Kingery and Bulmash interpolations are found to significantly underestimate peak overpressure and impulse values. Herein, all the blast scenarios

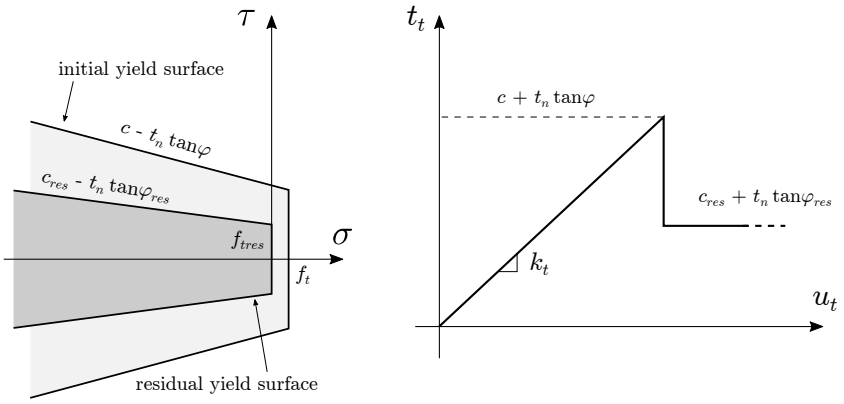

Figure 1: Initial and residual strength surfaces (left) and tangential stress-displacement relationship (right) used for modelling joints behaviour.

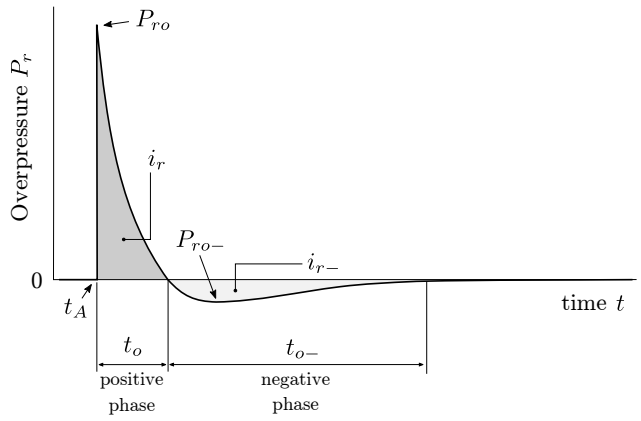

Figure 2: Time evolution of overpressure (i.e. the pressure measured relatively to the atmospheric one) due to an explosion acting on a target.

considered (Sect.s 4, 5, 6) are in the free-field (no confinement), involve scaled distances 0.65 m/kg$^{1/3}$ < Z < 3.97 m/kg$^{1/3}$, and no surfaces of reflection stand between the explosive material and the target. ConWep model is thus used.

Blast loads are computed through an external library which accounts for the effects of surface rotation of masonry components, change in incident angle, variation of the relative distance between explosive and blocks, and the deformability of the latter. At each time step, the history of the blast overpressure $P_r(t)$ is thus computed/updated according to the detonation time and point, the actual position and the angle of incident of the (centroid of the) impinged surfaces of blocks (at the level of the discretization in triangular elements). Herein the effects due to the angle incidence are modelled with the simplified approach implemented in ConWep [17]. Nevertheless, the external library can treat as well more realistic interpolations and account, in detail, for the effects of the incident angle, see e.g. the approach proposed in [48]. The external library is implemented in C++ language and Qt widget toolkit is used to realize the dynamic link with the DE Software [18]. Blast loads are applied and updated at each time step with appropriate algorithms (for rigid and deformable blocks) implemented in 3DEC FISH language.

4. Validation of the Discrete Element model

The proposed numerical model is herein compared and validated with existing experimental tests. Among the experiments available in the literature, we select one of the most well-documented [34]. Notice that performing blast experiments in either reduced- or full-scale presents many difficulties, due to the nature of the loading action, which may result in large uncertainties of the recorded results, hence demands repeated tests.

Michaloudis and Gebbeken [34] analysed the response of unreinforced masonry walls subjected to far-field and contact explosions through experimental and numerical investigations. Among four tests, two involved masonry walls which were subjected to the explosion of W_1 = 810 kg and W_2 = 1150 kg of TNT at R = 37 m from the targets, in the free-field (no confined explosions). No surfaces of reflection stand between the explosive material and the target. Due to the large stand-off distance, the blast wave impinges almost uniformly and simultaneously the entire target, without any other reflection taking place. Nevertheless, no information is given concerning the evolution of the blast pressure in the experimental tests. The brickwork consists of a running bond pattern with bricks of nominal dimensions $a \times b \times w$ = 80 × 240 × 120 mm, see Figure 3. The boundaries of the walls are constrained, through mortar interfaces, to stiff fixed supports.

In Test 1 (W_1 = 810 kg, R = 37 m), the observed maximum outward and inward deflection at the centre of the wall are 77 mm and 37 mm, respectively. In Test 2 (W_2 = 1150 kg, R = 37 m), a breach at the centre of the wall originates mainly due to joints failure. Failure within the body of individual bricks is not observed or is negligible [34]. The maximum dimensions of the breach are equal to 4 bricks along the length of the wall and to 13 bricks

along the height (see Fig. 6).

In the numerical Discrete Element (DE) model, a constant thickness of the mortar $h_m = 10$ mm is assumed, in the lack of more detailed information for the walls. Table 1 presents the material parameters of the numerical model, which have been selected from the literature, see e.g. [46, 58, 38]. We recall that subscript *res* identifies the residual (post-softening) value of the parameters (see Fig. 1). All the nodes of the edges of the surfaces at the boundaries are pinned. The blocks can thus only deform (no rotation is allowed). Blast loads are computed and applied using the dynamic library presented in Section 3.

From convergence analyses for contact and finite difference discretization (see [15, 32]), we find that at least 10 contact points along the wall's thickness (w in Fig. 3) are required to accurately modelling the out-of-plane deflection of the structure and avoid numerical artefacts. The finite difference mesh for deformable blocks is selected from mesh convergence analyses, see Fig 3 (cf. [32]).

4.1. Numerical results

We compare in Table 2 the numerical results obtained with the DE model and the test data [34] for Test 1 ($W_1 = 810$ kg, $R = 37$ m). The discrete approach predicts outward and inward deflections in agreement with the results in [34]; the relative error is within 3.24% the experimental values. It has to be emphasized that typical values for masonry properties were used in the DE model and no fitting was performed. We present in Figure 4 the time evolution of the numerically measured deflection at the centre of the wall. In the free-oscillating response, the system gradually dissipates energy as a result of the slip along interfaces, until equilibrium. A permanent outward deflection of approximately 7.1 mm at the centre is predicted by the model. No evidence is given in [34] concerning a permanent displacement.

For Test 2 ($W_2 = 1150$ kg, $R = 37$ m), we present in Figure 5 the out-of-plane response and the consequent formation of the breach from the numerical simulations. Figure 6 and Table 3 compare the breach dimensions of the numerical simulations with the experimental evidence. The DE model is found to capture the form of failure and the location of the breach. Nevertheless, a small difference in the number of the bricks that are removed from the wall is observable. This may be due to the fact that (*i*) complex fluid-structure interaction phenomena can take place during the explosion (and which are not considered in our simulations); (*ii*) in the test, some brick involved in the breach, even being few, break, which is not considered herein, and (*iii*) head joints in the tested wall have lower strength than the bed joints, due to the lack of the beneficial effect of gravity and construction habits.

5. Study of the dynamic response of a barrel vault subjected to a centred explosion

Once the proposed model has been validated, we perform numerical tests to investigate the response of an arched masonry structure, namely a barrel vault (see Fig. 7), subjected to a centred blast. DEM simulations are used here to understand the influence of various micro-mechanical parameters, such as the dilatancy and the building blocks size, on the dynamic response of the system.

5.1. Geometric model and discretization

The geometric model of the considered configuration is presented in Figure 7. The masonry bricks have size $a \times b \times w = 250 \times 296 \times 200$ mm. The thickness of the mortar is 10 mm. The vault has inner diameter $d_i = 2800$ mm, thickness w (outer diameter $d_e = 3200$ mm), and length $l = 3060$ mm. The longitudinal length of the structure has been selected upon considerations on the characteristic lengths associated to the blast wave and the hemispherical shock front.
The base ($y = 0$) and the edges ($z = 0$ and $z = l$) of the structure are assumed to be connected with fixed supports through contact interfaces (whose mechanical properties are assumed to be identical to the masonry joints). The supports have length $l_s = 150$ mm and thickness w. The fixed supports can represent various physical situations. For instance, they may designate the presence of rigid arched ribs or rigid walls at the lateral extremities of the vault. In addition, they could be used to approximate, to a certain degree, a vault, whose longitudinal length is much bigger than its diameter. The latter situation can be justified only for hemi-/spherical loads centred in the middle of the vault, as it is the case in this study at the beginning of the loading which coincides with the maximum pressure.

The contact discretization for the DE model is studied through two sets of analyses, which are fundamental for assuring reliable numerical results. First, in a quasi-static elastic calculation, the central layer of blocks is subjected to a constant and uniform pressure equal to 100 kPa acting on the inner faces. Differently from the previous simulations, herein mass damping is considered in order to dissipate oscillations and reach equilibrium fast. This first calculation allows to determine the fineness of the discretization of contacts along the circumferential and radial directions for each block (mesh convergence analysis). Second, the structure is subjected to the pressure of a surface blast $W = 10$ kg located at the ground ($y = 0$) and at the centre ($z = l/2$). No damping is considered. The deflection of different points at the vault's key is monitored to investigate the influence of the contact discretization along the longitudinal direction (z axis). On the basis of this mesh convergence analysis, the selected discretization consists of tetrahedra of average characteristic length equal to 35 mm, with $13 \times 6 \times 10$ contacts points along dimensions

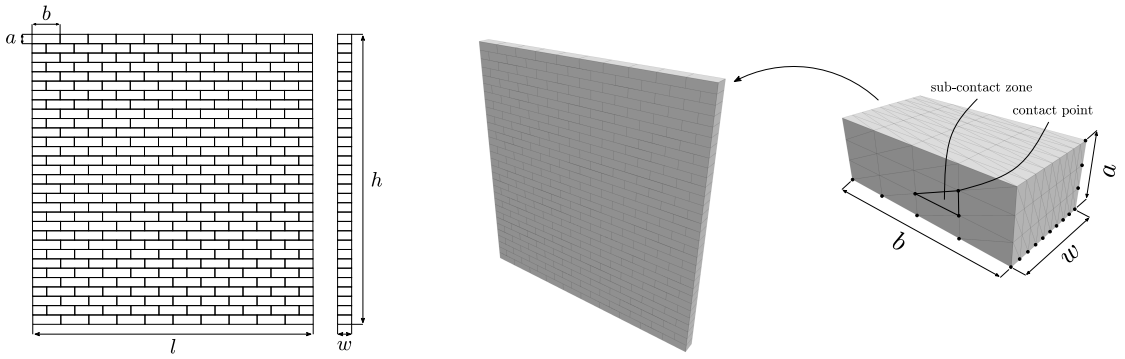

Figure 3: Geometric (left) and DE model (right) for test 1 and 2 in [34]. The masonry wall has thickness $w = 120$ mm, bricks have nominal size $a \times b \times w = 80 \times 240 \times 120$ mm.

Table 1: Material parameters of the numerical DE model.

Blocks properties			Joints properties					
density	(kg/m^3)	2470	k_n	(GPa/m)	50	c	(kPa)	500
E_b^*	(MPa)	5220	k_t	(GPa/m)	20.83	f_t	(kPa)	100
G_b^*	(MPa)	2170				c_{res}, $f_{t_{res}}$	(kPa)	0
						φ	(°)	30
						ψ	(°)	0

Table 2: Maximum outward and inward deflection at the centre of the wall for Test 1. Comparison between the observed values and the numerical predictions with the DE model.

Maximum deflection	Experiment	DEM
Outward (mm)	77.0	78.2
Inward (mm)	37.0	38.2

$a \times b \times w$, see Figure 8.
We present in Figure 9 the deformed shape, along the longitudinal direction, for the selected discretization, obtained at the equilibrium, under a static pressure of 100 kPa.

Once the appropriate discretization is selected, we proceed with the study of the behaviour of the barrel vault under explosive loads. In the first step, gravity is applied to the structure to reproduce the stress state within the vault under self-weight. The quasi-static equilibrium solution is

Table 3: Comparison of the breach dimension (height×width in terms of number of involved bricks) from the numerical results (DEM) and the experimental test.

Breach	Experiment	DEM
Dimensions	13×4	14×2
No. involved bricks	40	22

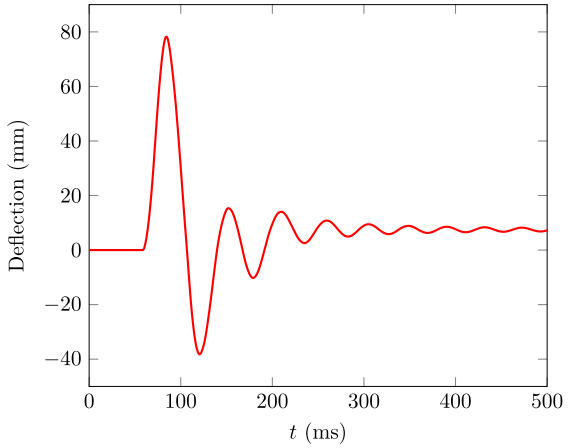

Figure 4: Time evolution of the deflection at the centre of the wall from the numerical DE simulations of Test 1 ($W_1 = 810$ kg, $R = 37$ m).

used as the initial state for the simulation of the response to a surface blast due to a TNT explosive weight $W = 10$ kg, located at the centre ($y = 0$, $z = l/2$). The considered blast scenario corresponds to a moderate-field explosion. The best-fit interpolations used [21] allows usually to be on the safety side. The elastic parameters for blocks and joints are presented in Table 4. In paragraph 5.2 we investigate the influence of the associativity of the sliding behaviour of masonry joints and the combined effects of friction and dilatancy angles in paragraph 5.3. Different

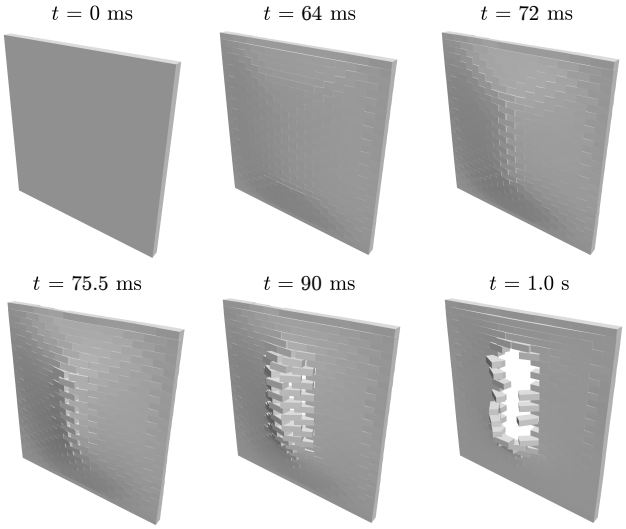

Figure 5: Response of the DE model for Test 2 (W_2 = 1150 kg, R = 37 m).

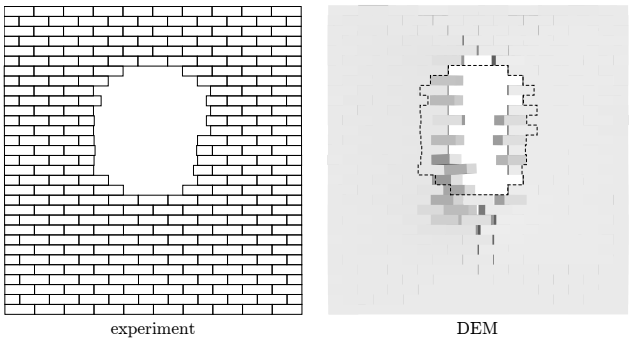

Figure 6: Comparison between the experiment (left) and the numerical DEM results (right) for Test 2 (W_2 = 1150 kg, R = 37 m). The experimental breach extension is schematically represented by the black dashed line.

values of cohesion and tensile strength of the interfaces and their dependency on the structural strength of the system are explored in paragraph 5.4. Finally paragraph 5.5 examines the role that the size of the building blocks plays in the dynamic response.

5.2. The effect of associative or non-associative friction

The influence of the associativity of the masonry joints behaviour is studied, assuming zero cohesion and zero tensile strength for the joints. A constant angle of friction of both the head and bed joints is considered (cf. Fig. 8), namely $\varphi^b = \varphi^h = 35°$ (superscripts b and h refer to bed and head joints, respectively).

Figure 10 presents the time response in terms of the deflection at different points located at the vault's key (with reference to Fig. 8), assuming an associative sliding behaviour, i.e., equal friction and dilatancy angles, $\varphi^h = \varphi^b = \psi^b = \psi^h = 35°$. The time history of the loading is

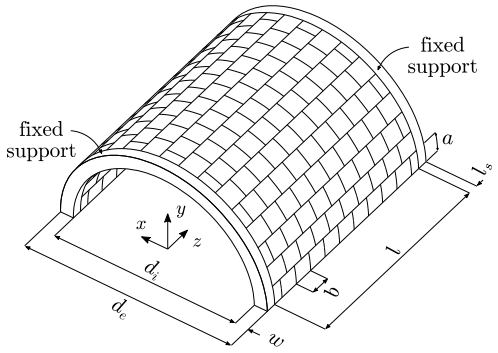

Figure 7: Geometric model of the masonry barrel vault under investigation. Bricks have size $a \times b \times w$ = 250×296×200 mm. The vault has inner diameter d_i = 2800 mm, thickness w (outer diameter d_e = 3200 mm), and depth l = 3060.

Table 4: Material parameters used in the numerical simulations of the masonry barrel vault.

Blocks properties			Joints properties		
density	(kg/m^3)	2000	k_n	(GPa/m)	100.0
E_b^*	(GPa)	14.5	k_t	(GPa/m)	41.7
G_b^*	(GPa)	6.0			

presented, for the same locations, in Figure 11 and Table 5.

The blast overpressure, acting on the inner face of the vault, causes an initial outward slip (≈ 1 mm) of the masonry blocks. The elements at the boundaries partially rotate around the rigid supports, while the longitudinal layers of blocks begin to deflect in the outward direction (see Fig. 12). Nevertheless, the relative confinement of the vault (due to the presence of the fixed supports and the dilatant behaviour of interfaces) results in a limited in-plane response. Membrane compressive forces develop in the plane of the vault, along the longitudinal direction, giving rise to so-called arching actions. The resulting response of the structure is similar to the one of an arching wall (between supports that restrain the outward movement) subjected to out-of-plane loads [13]. Each layer of bricks along the longitudinal axis develops compressive arching actions (see Fig. 12), while the in-plane response is limited.

The presence of travelling stress−bending and compressive/tensi internal to the structures, which are further reflected at the boundaries makes the displacements of the masonry blocks (cf. Fig. 10) to oscillate and move outward. This is a direct consequent of the aforementioned arching mechanism. The concurrent dilatant behaviour of the masonry interfaces, which increases the membrane compressive forces, the geometry of the structure, and the presence of infinitely rigid supports oblige the structure to find a new equilibrium point towards positive deflections.

When a non-associative behaviour with zero dilatancy is considered, the resistance of the structure is found to

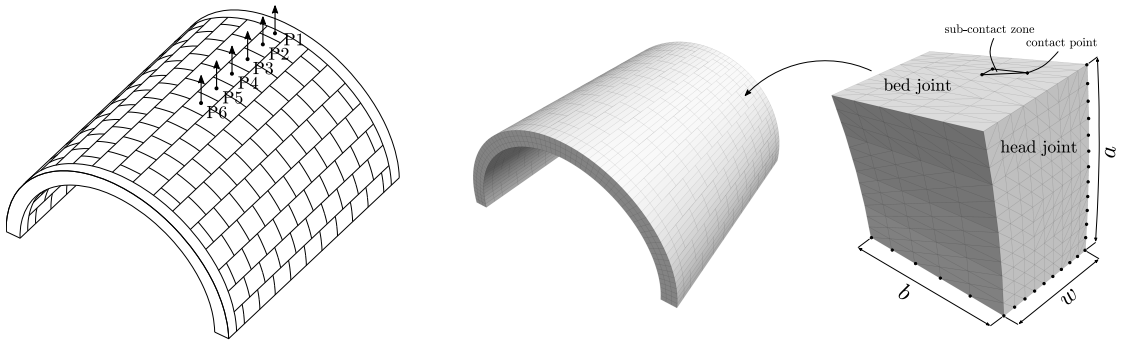

geometric model DE model

Figure 8: Geometric model of the masonry barrel vault (left), with highlighted monitoring points used in the following simulations, and Discrete Element model with contact discretization and finite difference mesh of the blocks (right).

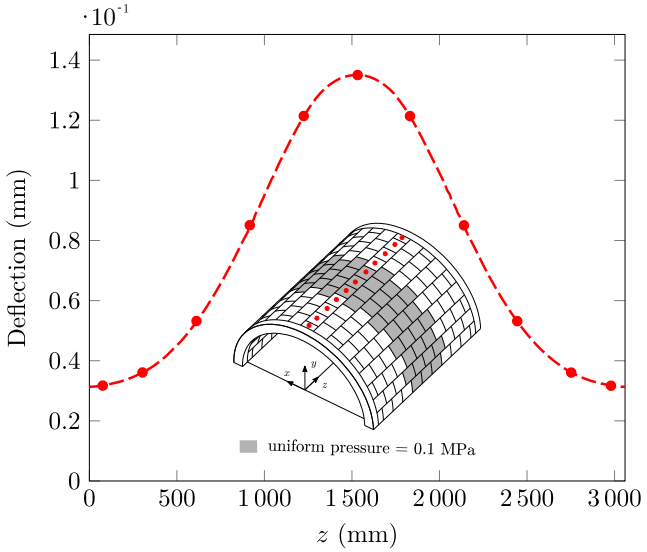

Figure 9: Deformed shape, along the longitudinal direction, at the key's vault under a constant pressure of 100 kPa applied to the region highlighted in grey. The circles represent the blocks' centroids. An elastic behaviour is assumed for the masonry joints.

decrease, as a consequence of the reduced membrane compressive stress (zero dilatancy) that reduces the apparent friction between the blocks in the longitudinal direction (z axis). Consequently, the arching mechanism is reduced as well. We present in Figure 13 the displacement history measured at the vault's key for the case of associative and non-associative (with zero dilatancy) sliding behaviour. The maximum deflection measured in the associative case is found to be 14% smaller than the one obtained with a non-dilatant sliding behaviour, as presented in Table 6. As also noticed in [15], joints showing zero dilatancy reduce considerably the stress in masonry. In this case, a non-associative sliding behaviour ($\psi^b = \psi^h = 0°$) results in a reduction of approximately 85 % of both normal and shear stress at the joints and 50% of the maximum principal stress within the masonry blocks.

Differently from the above case, the outward oscillations of the blocks, due to the presence of internal travelling stress waves, reflected at the boundaries, does not result in increased compressive membrane forces (lack of dilatancy). The deflection at the vault's key displays a second peak which is much higher due to the apparent frictional resistance at the edges which is lower compared to the associative one. This counter-intuitive result is due to the presence of elastic waves in the structure which lead to the progressive development of additional frictional slip in the case of the non-associative case which is more prone to frictional slip. These waves are trapped in the structure due to the rigid supports that reflect them and are dissipated through frictional slip.

Table 5: Overpressure peak, P_{ro}, underpressure peak, P_{ro-}, arrival time of the shock wave, t_A, positive phase duration, t_o, and negative phase duration, t_{o-}, due to 10 kg of TNT predicted by the model at different points located at the vault's key (refer to Fig. 8).

location	P_{ro} (MPa)	P_{ro-} (kPa)	t_A (ms)	t_o (ms)	t_{o-} (ms)
P6	23.08	-8.40	0.48	0.97	1.52
P5	21.54	-4.93	0.50	1.05	1.41
P4	18.48	-1.27	0.56	1.24	1.13
P3	14.87	-0.14	0.65	1.63	0.61
P2	11.77	-0.01	0.78	2.28	0.34
P1	9.52	0.0	0.91	2.98	0.0

Table 6: Dilatancy ψ^b and friction angle φ^h considered in the parametric study and related maximum deflection observed in the masonry vault. The results refer to $\varphi^b = 35°$, $\psi^h = 0°$, and $f_t = c = 0$ MPa.

sliding behaviour	$\varphi^b = \varphi^h$ (°)	$\psi^b = \psi^h$ (°)	Maximum deflection (mm)
associative	35	35	55.80
non-associative	35	0	65.04

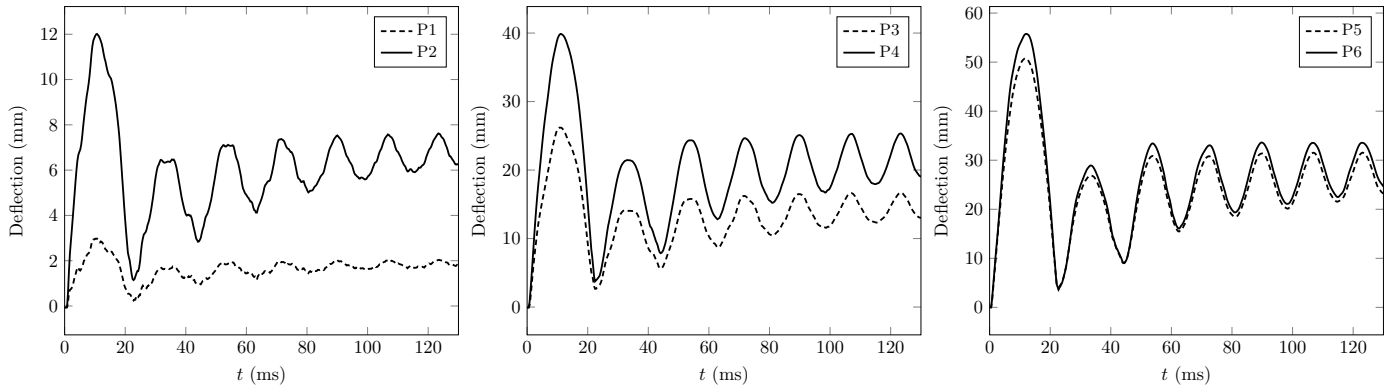

Figure 10: Response of a barrel vault subjected to 10 kg of TNT in terms of the deflection of different points located at the vault's key. The results are for $\varphi^h = \varphi^b = 35°$, $\psi^b = \psi^h = 35°$, $f_t = c = 0$ MPa.

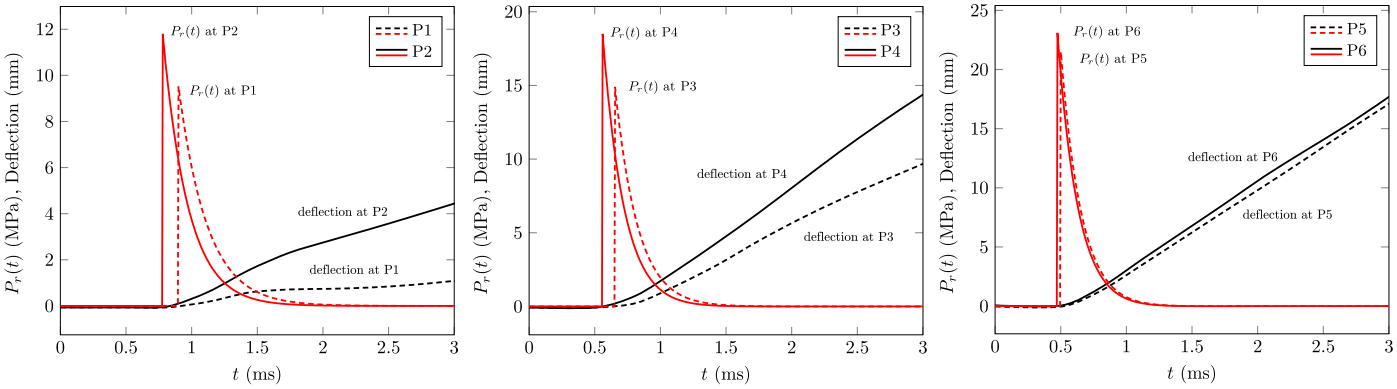

Figure 11: Overpressure profiles due to 10 kg of TNT at the vault's key, see Fig. 10.

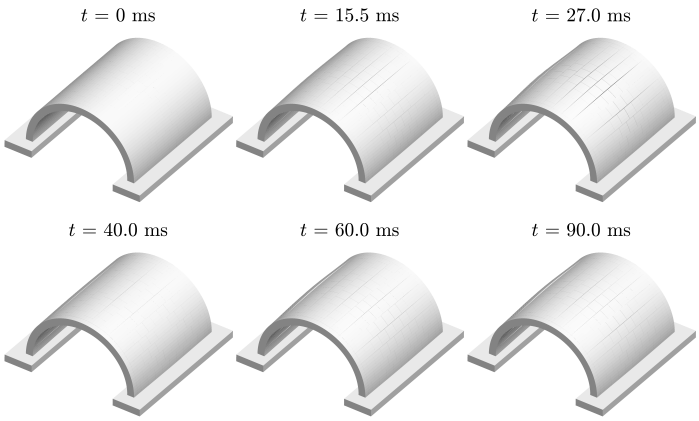

Figure 12: Evolution of response of a barrel vault subjected to 10 kg of TNT and formation of the arching mechanism. The results refer to $\varphi^h = \varphi^b = 35°$, $\psi^b = \psi^h = 35°$, $f_t = c = 0$ MPa.

5.3. Friction and dilatancy effect for non-associative friction

The effects of a non-associative behaviour, with varying dilatancy, and of the friction angle of the joints are explored. For the bed joints, we consider a constant angle of friction, i.e., $\varphi^b = 35°$, while the dilatancy angle varies between 0° and 35°. At the interfaces representing the head joints, the influence of different values of the friction angle, φ^h, (and zero dilatancy) is explored. The choice originates from the fact that head joints usually are weak planes in masonry structures, due to the lack of gravity during the construction process. This stands also for the bed joints whose lying plane makes an angle less than 90° with the direction of applied gravity. Nevertheless, we neglect this latter condition herein. Table 7 presents the considered values of the dilatancy and the friction angle, as well as the maximum deflection numerically measured within the structure.

At varying of the friction angle, φ^h, arching actions still develop, but to a gradually reduced extent, see Fig. 14. As expected, the smaller the friction angle is, the larger the slippage observed between adjacent blocks becomes. This is clearly visible at the supports, point P1 (Fig. 14). In fact, low angles of friction prevent the formation of membrane compressive stress, hence of an effective and beneficial arching mechanism. This is shown in Figure 15 which depicts the response of the structure for $\varphi^h = 10°$, $\varphi^b = 35°$, and $\psi^b = \psi^h = 0°$.

Table 7 and Figure 17 present the maximum deflection observed in the masonry vault for different angles of friction, φ^h, and dilatancy, ψ^b. Collapse is considered when a maximum deflection equal to 200 mm, i.e., the thickness of the vault, is developed. The response of the system is

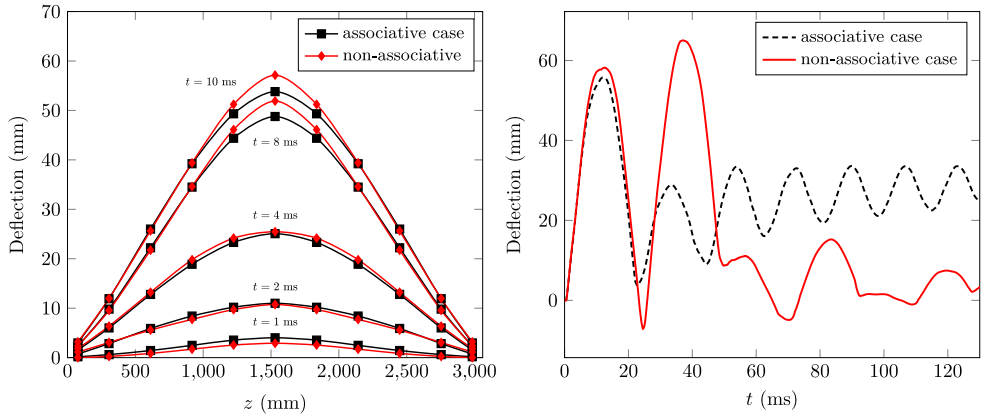

Figure 13: Response of a barrel vault subjected to 10 kg of TNT in terms of the deformed shape at vault's key (left) and deflection at point P6 (right) for a dilatant behaviour of the masonry joints and assuming a non-associative sliding behaviour ($\psi^b = \psi^h = 0°$). The results are for $\varphi^h = \varphi^b = 35°$, $f_t = c = 0$ MPa. The blast parameters are those shown in Table 5.

Table 7: Dilatancy ψ^b and friction angle φ^h considered in the parametric study and related maximum deflection observed in the masonry vault. The results refer to $\varphi^b = 35°$, $\psi^h = 0°$, and $f_t = c = 0$ MPa.

ψ^b (°)	φ^h (°)	Maximum deflection (mm)	ψ^b (°)	φ^h (°)	Maximum deflection (mm)
0	35	65.04	2	10	86.71
	20	63.45		5	> 200
	15	66.24		0	> 200
	10	86.86			
	5	> 200			
	0	> 200			
5	10	86.66	10	10	86.57
	5	> 200		5	> 200
	0	> 200		0	> 200

found to depend only on the friction angle, while the effect of bed joints dilatancy angle on the maximum deflection is negligible. It is worth noticing the presence of a roughly estimated collapse displacement capacity, i.e. the maximum out-of-plane deflection that the system can withstand. This can be clearly seen for the case with $\psi = 0°$, for which the effects of the friction angle φ^h are widely investigated. For angles $\varphi^h \geq 15°$, the numerically measured maximum deflection remains almost constant, $u_{max} \approx 60$ mm. For $\varphi^h = 10°$, the displacement increases by 20 %, i.e., $u_{max} = 87$ mm, and collapse occurs at smaller angles of friction. The definition of a collapse displacement capacity is usually applied to out-of-plane load bearing walls and it can be roughly estimated as half of the wall thickness, $u_{max} \approx w/2$, see e.g. [36] and [35]. The numerical results for the barrel vault (Fig. 17) seem to corroborate that the same stands for an arched structure like a barrel vault, i.e., $u_{max} \approx w/2 \approx 100$ m.

Figure 16 displays the time-evolution of the out-of-plane displacement in function of the dilatancy angle of the bed joints, ψ^b, and for constant friction angles $\varphi^b = 35°$ and $\varphi^h = 10°$. We clearly notice that the first-peak deflection does not depend on the value of the joints dilatancy. Nevertheless, the dynamic response, i.e., the evolution in time of the deflection, is influenced by the dilatant behaviour of the joints, but only slightly. In particular, an increase of the post-peak deflection is observed for higher dilatancy. Indeed, the larger the dilatancy of the interfaces is, the higher the transmitted compressive thrust is and the lower the sliding becomes.

5.4. Cohesion and tensile strength effect

The effect of the cohesion and tensile strength of the bed joints is herein investigated considering $\varphi^b = 35°$ and $\varphi^h = 10° - 5°$, and zero dilatancy $\psi^b = \psi^h = 0°$. The case with $\varphi^h = 10°$ is selected in order to investigate the effects on the dynamic response. Indeed, for the same value of the friction angle and zero cohesion and tensile strength, the vault does not undergo collapse (cf. Tab. 7). The influence of the two strength parameters on the failure mode and collapse capacity of the structure is instead investigated for $\varphi^h = 5°$ (collapse for $f_t = c = 0$ MPa, cf. Tab. 7). The selected combinations of values for cohesion and tensile strength are presented in Table 8. Once the onset of tensile and/or shear failure is reached, the residual values of cohesion and tensile strength are imposed to be zero (see Fig. 1). Zero cohesion and zero tensile strength are assumed for the head joints.

Figure 18 shows the response of the system for $\varphi^h = 10°$ and a wide range of the value of the strength parameters. We notice that both cohesion and tensile strength do not influence the first-peak response of the structure. Only the post-peak response slightly depends on the two parameters, due to the increased/reduced amount of the number of joints that underwent softening. This holds true since

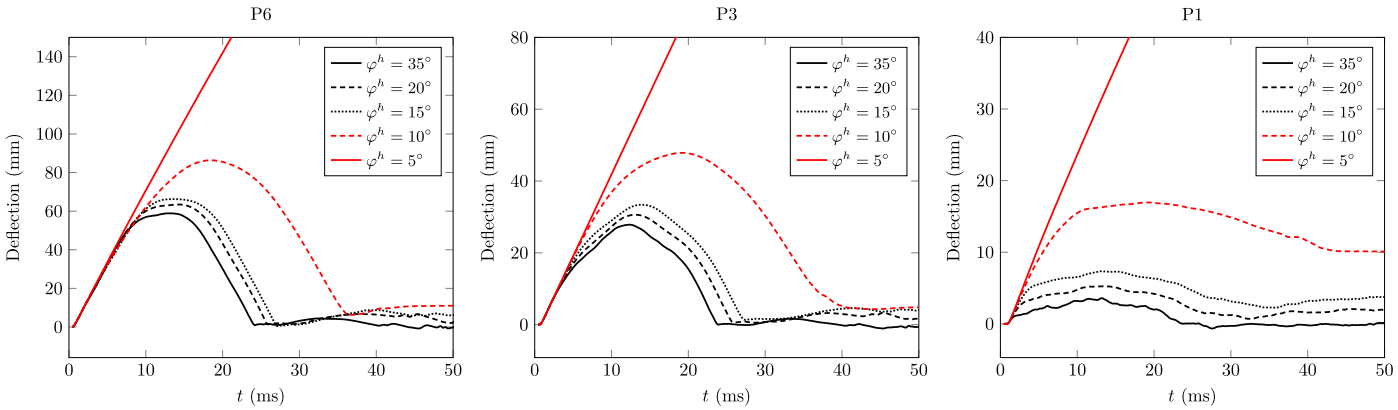

Figure 14: Influence of the head joints angle of friction, φ^h, on the dynamic response of a barrel vault subjected to 10 kg of TNT in terms of the deflection of different points (P6, P3, and P1 cf. Fig. 8). The results refer to $\varphi^b = 35°$, $\psi^b = \psi^h = 0°$, and $f_t = c = 0$ MPa.

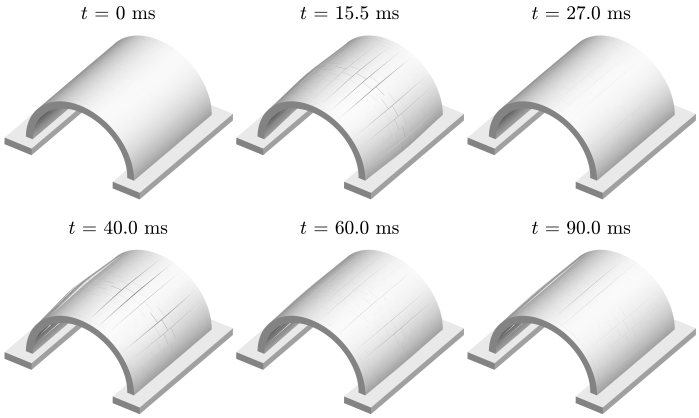

Figure 15: Evolution of response of a barrel vault subjected to 10 kg of TNT. The results are for $\varphi^b = \varphi^h = 35°$, $\psi^b = \psi^h = 0°$, and $f_t = c = 0$ MPa.

Table 8: Cohesion c and tensile strength f_t considered in the parametric study and related maximum deflection observed in the masonry vault for $\varphi^b = 35°$, $\psi^b = \psi^h = 0°$. The residual values are kept constant $c_{res} = f_{t\,res} = 0$ MPa.

f_t (MPa)	c (MPa)	Maximum deflection $\varphi^h = 5°$ (mm)	Maximum deflection $\varphi^h = 10°$ (mm)
0	0	> 200	86.86
	0.1	> 200	86.57
	0.5	> 200	86.55
0.1	0.5	> 200	86.29
0.5	1.5	> 200	86.29
1.5	3.0	> 200	86.29

the dynamic response is strongly influenced by the relative slip that takes place at the head joints along the longitudinal direction (z axis), for which zero cohesion and tensile strength are always assumed.

In the case of $\varphi^h = 5°$, the system's failure mode and collapse capacity are found to be independent from the value of tensile strength and cohesion, see Table 8.

5.5. Building blocks size effect

The size of the building blocks can influence the compression and the shear strength of the structure, as well as its stiffness [37] and inertia [33]. Several are the reasons of the scale effects of the building blocks. Among those, the number of joints in the structure is usually the leading parameter that influences the dynamic response, energy dissipation due to friction, and overall strength.

We present herein numerical analyses to asses the building blocks scale effect, for some sets of material parameters used in paragraphs 5.2 and 5.3.

We investigate the behaviour of the vault using blocks that are half and twice their original size, assuming constant overall thickness $w = 200$ mm (see Fig. 19) and mortar height $h_m = 10$ mm.

Table 9 and Figure 20 present the maximum deflection that was reported within the vault for different values of the dilatancy and friction angles and highlight the importance of the horizontal joints.

The system with half the blocks size displays an increase in the overall outward deflection of the structure due to the larger number of interfaces in the system. It is worth noticing that the mortar thickness is assumed to be the same in each model, thus the normal and tangential stiffness, k_n and k_t, are kept the same between the models, cf. Eq. (2). Therefore, the larger number of masonry joints results in a decrease of the overall flexural stiffness of the structure.

Similarly to what observed in paragraph 5.2, masonry joints with zero dilatancy result in an enhanced out-of-plane response also for blocks that are half the reference size (the maximum deflection is 9% larger than the one related to the associative case). Moreover, the zero dilatancy joints display reduced stress (90 % of compressive stress and 92 % of shear stress) with respect to the associative case.

The model with twice the blocks size displays smaller

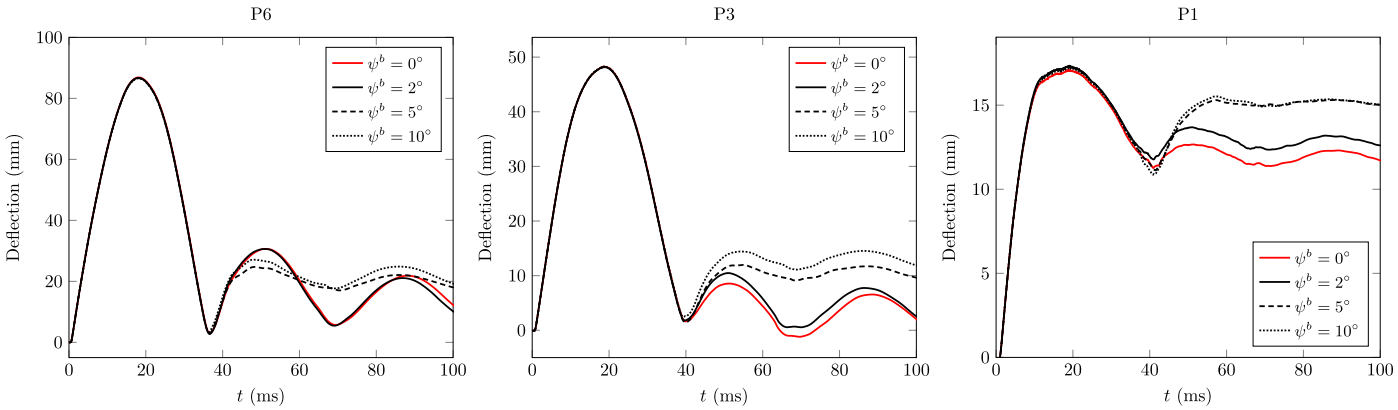

Figure 16: Influence of the bed joints dilatancy, ψ^b, on the dynamic response of a barrel vault subjected to 10 kg of TNT in terms of the deflection of different points (P6, P3, and P1 cf. Fig. 8). The results refer to $\varphi^b = 35°$, $\varphi^h = 10°$, $\psi^h = 0°$, and $f_t = c = 0$ MPa.

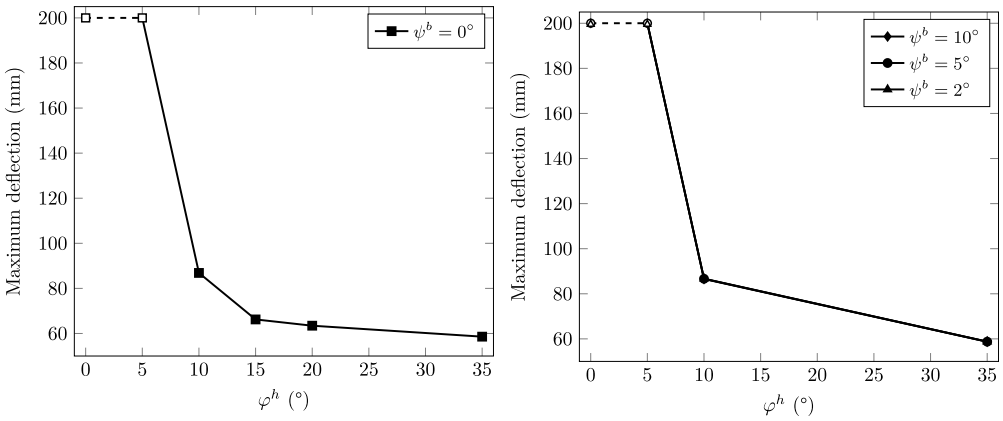

Figure 17: Maximum deflection observed in the masonry vault at varying of φ^h and ψ^b ($\varphi^b = 35°$, $\psi^h = 0°$, $f_t = c = 0$ MPa).

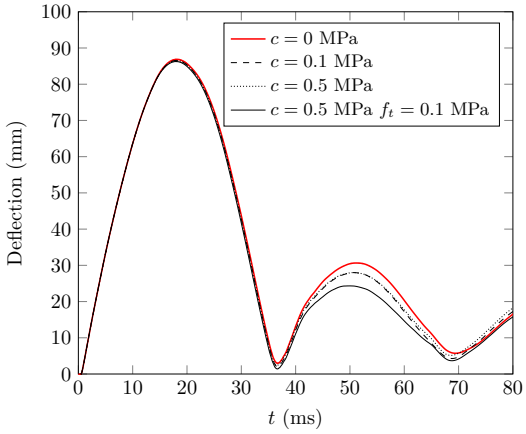

Figure 18: Time evolution of the deflection at the centre of the vault's key for different combinations of cohesion and tensile strength of the interfaces.

out-of-plane displacements and reduced bending, if compared to the reference blocks size, for the case $\varphi^b = \varphi^h = 35°$. The reason lies on the same consideration made for the half blocks size: larger blocks result in higher flexural stiffness. Figure 21 displays the dynamic response for different building blocks sizes assuming (a) an associative sliding behaviour and (b) zero dilatancy masonry joints. Also in the case of double blocks size, the non-associative sliding behaviour corresponds to increased out-of-plane displacements (the maximum deflection is found to be 12% larger than the associative case) and reduced stress in the masonry (namely, the compressive stresses are reduced to the 96 % while the shear stress to the 95 % of the ones corresponding to an associative behaviour).

For $\varphi^b = 35°$ and $\varphi^h = 10°$ (see Tab. 9), we find that the model with double blocks size displays larger deflections, with respect to the reference size. Indeed, an increase in the blocks dimensions corresponds to a decrease of the number of masonry joints, which further gives smaller overall plastic dissipation, namely friction work, and larger relative slippage. In particular, the total friction work with double blocks size is approximately 50% smaller than the one corresponding to the model with half blocks size, see Fig. 22.

6. Rigid vs deformable blocks. Is a rigid blocks assumption always appropriate?

Herein we investigate the simplified modelling assumption of infinitely rigid blocks which is often preferred in

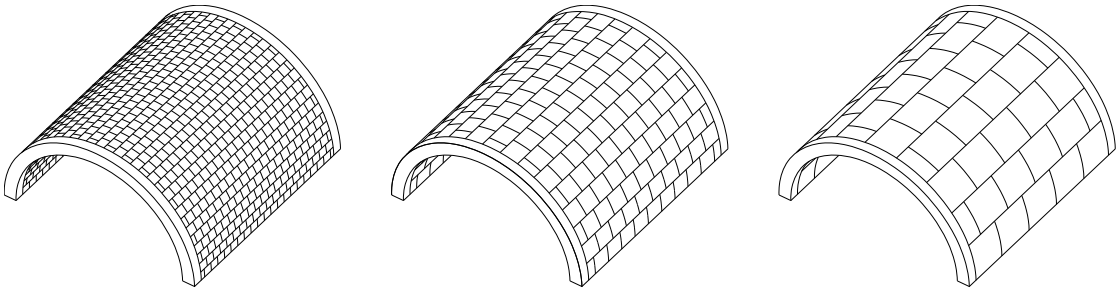

Figure 19: The building blocks size effect is investigated using blocks that are half and twice their original size, assuming constant overall thickness $w = 200$ mm and mortar height $h_m = 10$ mm.

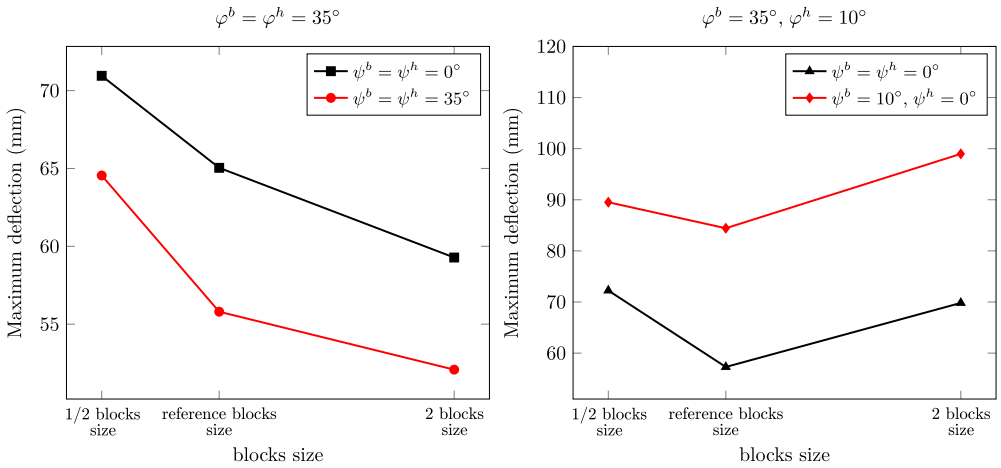

Figure 20: Comparison of the maximum deflection observed in the masonry vault for different size of the building blocks, with $\varphi^b = \varphi^h = 35°$ (left) and $\varphi^b = 35°$, $\varphi^h = 10°$ (right). The results are for $f_t = c = 0$ MPa.

Table 9: Building blocks size effect on the maximum deflection observed within the structure. The results refer to $f_t = c = 0$ MPa.

φ^b (°)	φ^h (°)	ψ^b (°)	ψ^h (°)	Maximum deflection 1/2 bocks size (mm)	reference blocks size (mm)	2 blocks size (mm)
35	35	35	35	64.55	55.80	52.08
		0	0	70.95	65.04	59.29
35	10	10	0	121.95	53.62	71.51
		0	0	126.97	86.86	71.55

the literature, see e.g. [4, 2, 10, 15], because of its reduced computational cost with respect to the more detailed model with deformable blocks we are using herein. Under in-plane conditions, the rigid blocks assumption is usually reasonable under relatively low compressive loads, where the deformation is principally concentrated at the interfaces [45]. Nevertheless, for masonry structures subjected to out-of-plane loading, like those due to a blast, a rigid blocks model may give unrealistic results, see e.g. [35, 32].

Here we provide comparisons between rigid and deformable blocks models of the arched geometry previously investigated.

As mentioned in Section 5, several contact points through the thickness of the masonry structure undergoing out-of-plane displacement are required both for rigid and deformable blocks models (see also [23, 24, 15, 32]). However, in a rigid block model, the stress distribution at the interfaces is linear. Consequently, an accurate discretization of contacts is fundamental. For instance, it has been proved that in the frame of the DEM code herein used, 3DEC, at least 3 contact points along the thickness are required to obtain a satisfactory representation of the bending stiffness [24].

With rigid blocks, the normal and tangential stiffness (k_n and k_t, respectively) of the interfaces are modified with respect to the expressions previously derived (see Sect. 2) to account for the deformability of the blocks in the real structure (see also [31]):

$$k_n = \frac{E_b E_m}{E_b h_m + E_m h_b}, \tag{13}$$

$$k_t = \frac{G_b G_m}{G_b h_m + G_m h_b}. \tag{14}$$

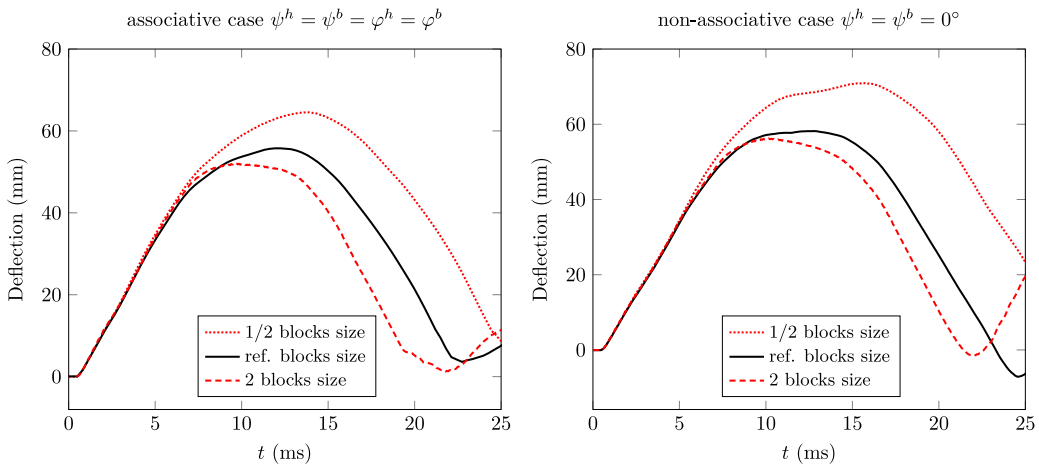

Figure 21: Comparison of the response of the masonry vault in terms of deflection at the centre of the vault's key (right, P6, cf. 7) for different size of the building blocks. The results are for $\varphi^b = \varphi^h = 35°$ and $f_t = c = 0$ MPa.

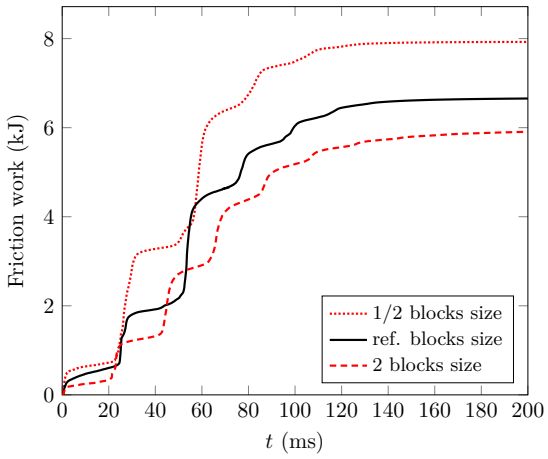

Figure 22: Time-history of joints friction work for different blocks size. The results are for $\varphi^b = \varphi^h = 35°$, $\psi^b = \psi^h = 0°$, and $f_t = c = 0$ MPa.

The elasticity lumping formulae (13) and (14) are derived for in-plane loading of planar structures [42]. For head joints, the block thickness h_b represents the brick length, while for bed joints, h_b is the brick height.
Table 10 displays the material elastic parameters used for the model with rigid blocks, derived from those given in Table 4 (for deformable DE) and considering the non-deformability of the blocks, see Eq.s (13, 14). The material parameters that define the plasticity behaviour and the corresponding softening remain unchanged, see Sect. 2. The fineness of the contacts discretization is investigated following the same approach used for deformable blocks (see Sect. 5, paragraph 5.1). The selected discretization consists of 5×4 (thickness $\times$ width) contact points at each masonry joint.

6.1. Rigid vs deformable blocks under quasi-static conditions

A constant uniform pressure equal to 100 kPa is applied to a central layer of the barrel vault (see Fig. 9). We assume a linear elastic behaviour of the interfaces for both models as in the case with deformable blocks (par. 5.1). Mass proportional damping is used (in this paragraph) to dissipate oscillations and reach equilibrium fast.
Figure 23 displays the deformed shape obtained at the equilibrium, using rigid and deformable blocks, respectively.

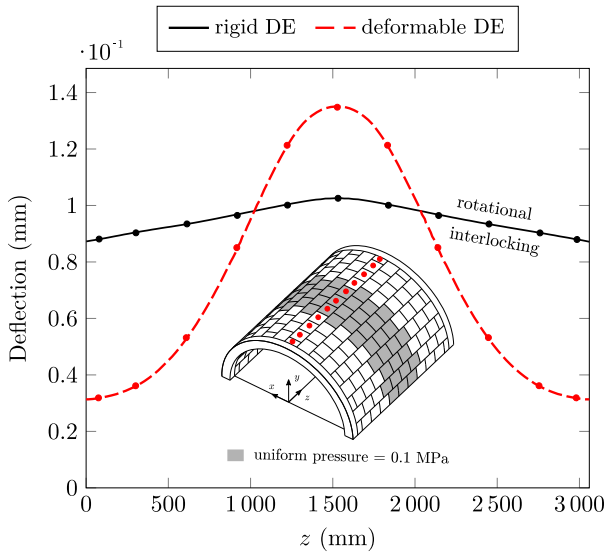

Figure 23: Comparison of the discrete element model with deformable and rigid blocks under a constant pressure 100 kPa applied to the region highlighted in grey. An elastic behaviour is assumed for the masonry joints.

The models with rigid and deformable blocks display different deformation modes and stiffness. In particular, the rigid blocks model shows a very high bending stiffness. This is due to the fact that the rigid discrete elements

Table 10: Material parameters used in the numerical simulations of the masonry barrel vault using a rigid block model. Superscripts b and h refer to bed and head masonry joints, respectively.

Blocks properties			Joints properties					
density	(kg/m^3)	2000	k_n^b	(GPa/m)	36.0	k_n^h	(GPa/m)	32.0
			k_t^b	(GPa/m)	15.0	k_n^h	(GPa/m)	13.4

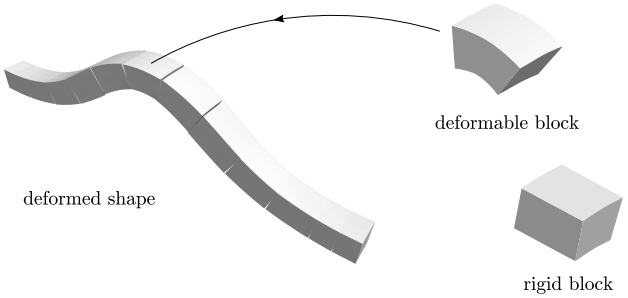

Figure 24: Out-of-plane deformation mode of blocky structure, modelled with deformable blocks (left). Block bending modes (right) with deformable (top) and rigid (bottom) blocks.

have infinite bending stiffness (i.e., non-deformable), as illustrated in Figure 24. As a result, a pure shear mode of deformation is observed. The rigid model is affected by what we define here as rotational locking; an artefact that can be quite important under out-of-plane loads leading to artificially high bending stiffness, as shear locking does in the Finite Element method.
We emphasize that the rotational locking is not a related to the lumping of elasticity at the interfaces, as performed in the rigid blocks model. Indeed, using building blocks that are half and twice their original size (refer to Fig. 19, paragraph 5.5), for both rigid and deformable block models, we obtain results comparable to those showed in Figure 23.

6.2. Rigid vs deformable blocks under blast actions

We explore here the adequacy of a rigid blocks assumption under blast actions. In particular, we are interested in analysing the effects of rotational locking on bending nonlinear eigenmodes, accounting for the shear- and tensile-failure at the masonry interfaces. No damping is considered.

We assume zero cohesion and tensile strength, $f_t = c = 0$ MPa, constant angle of friction of the joints, $\varphi^b = \varphi^h = 35°$, and either an associative sliding behaviour ($\psi^b = \psi^h = \varphi^b = \varphi^h$) or zero dilatancy joints, $\psi^b = \psi^h = 0°$.

In Figure 25 we compare the evolution of the deformed shape for both rigid and deformable blocks models subjected to 10 kg of TNT. When an associative behaviour of the interfaces is assumed, the overall response predicted by rigid DE is tantamount to the one obtained with deformable ones. The relative error is within 2.7%, see Table 11. The dilatant behaviour of the interfaces increases the local contact pressure which results in increase bending stiffness (for both models).

For zero dilatancy masonry joints, the rigid blocks model response is found to highly differ from the one predicted by the deformable DE model. Rotational locking (infinite bending stiffness) is at the origin. The rigid blocks model displays shear failure of the interfaces of the central (rigid) block and at the boundaries (see Fig. 25). The central block presents a time-lag in deflection compared to its adjacent blocks from the very beginning. This ultimately leads to the loss of any arching mechanism (differently to what observed with deformable blocks). Figure 26 depicts the different deformed shapes obtained with the rigid and deformable models. For the non-associative case, the rigid blocks predict a maximum deflection which is approximately 30% larger.

6.2.1. Influence of the building blocks size

We explore the effects of rotational locking at varying of the building blocks size.
Table 12 presents the maximum deflection measured within the structure for friction angle $\varphi^b = \varphi^h = 35°$. The results obtained with infinitely rigid blocks and their relative error are also shown.

We find that the rotational locking phenomenon influences the rigid blocks model, independently from the size of the building blocks. Nevertheless, major differences between deformable and rigid blocks are found for bricks of twice the original size. The associativity or not of the sliding behaviour of the masonry joints is, once again, found to affect the rigid model predictions, even if to a smaller extent with respect to the reference block size.

The simplified assumption of rigid blocks for blocky confined structures undergoing out-of-plane deformation is thus found to perform poorly under both quasi-static and fast-dynamic loads (independently from the size of building blocks), for the scenarios here considered.

7. Concluding remarks

The dynamic behaviour of masonry structures subjected to blast actions was studied here. For this purpose, a numerical model based on the DEM was presented and validated on the basis of recent existing, detailed experimental tests involving planar geometries subjected to far-field explosions. The essential features of the mechanical response

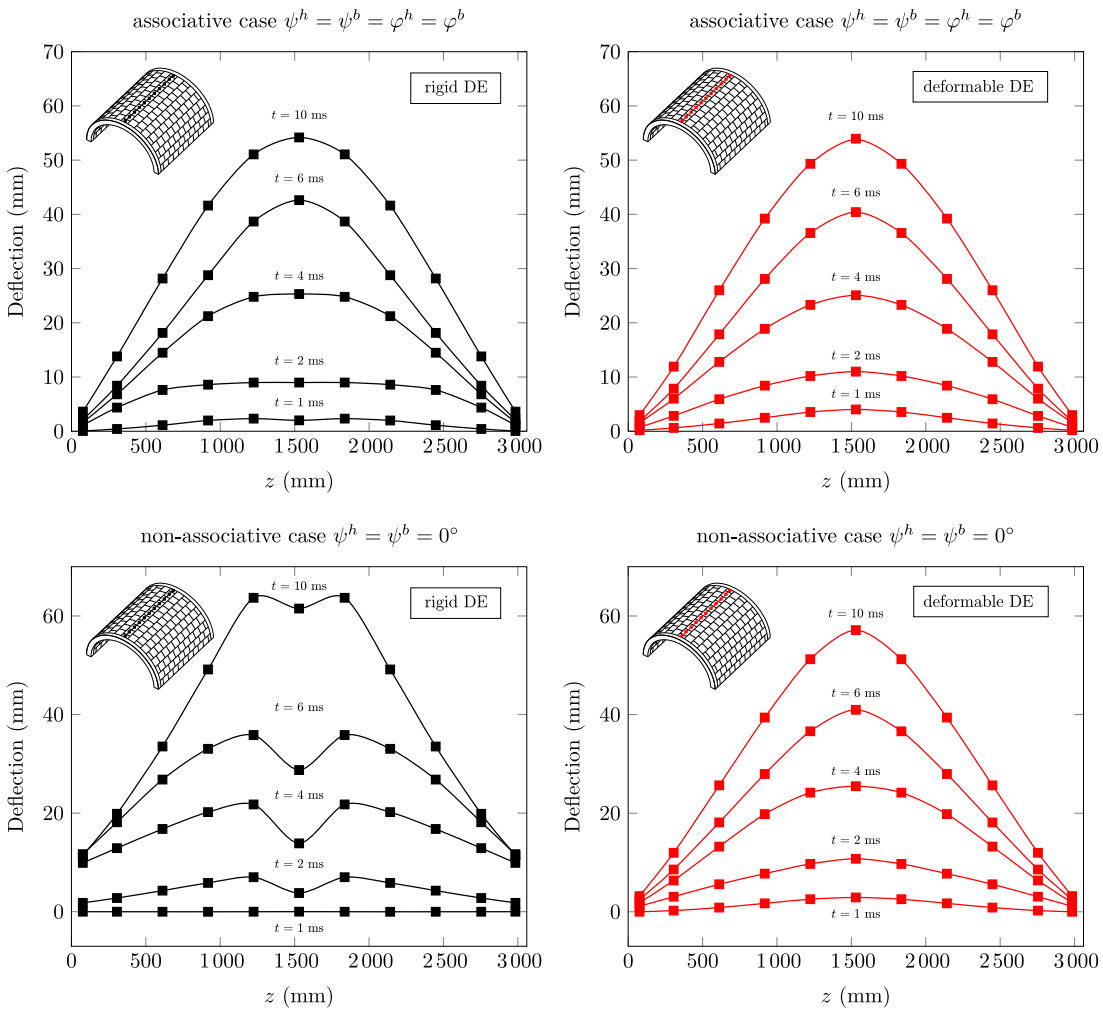

Figure 25: Evolution of the deformed shape, along the longitudinal direction, at the key's vault of the masonry vault subjected to 10 kg of TNT, obtained with rigid blocks (left) and deformable ones (right).

and failure modes were captured by the numerical model.

Once the numerical model was validated, it was used to assess the response of a curved masonry element, a barrel vault, to a centred blast. This kind of structure is of particular interest due to the interplay between membrane (in-plane) and bending (out-of-plane) modes of deformation and failure. The mechanical behaviour and out-of-plane response were investigated through detailed parametric studies in order to assess the most dominant parameters. Here we examined the influence of micro-mechanical parameters such as the joints' dilatancy and friction angle, the cohesion and tensile strength of the mortar joints, as well as the size of the building blocks. Typical values or range of values for masonry were considered for the above mentioned parameters.

For the numerical examples that were investigated, it was shown that the response of a barrel vault restrained to fixed supports is similar to that of a planar wall subjected to out-of-plane loads, confined to supports that prevent outward movement. Under the action of blast loads, membrane compressive forces develop and the longitudinal layers of brick bend, giving rise to an arching mechanism. Masonry joints with zero dilatancy (non-associative plastic behaviour) lead to reduced membrane forces, hence to an increase in out-of-plane deflections of the structure (14 % larger with respect to the associative case). Moreover, we showed that zero dilatancy of joints decreases the stress in the masonry ($\approx$ 85 % within the interfaces and $\approx$ 50 % within the blocks). This is not a surprising result but its quantification through our analyses shows the importance of non-associativity in the investigation, modelling, and design of masonry structures. This limits the application of conventional analysis tools of plasticity theory, such as limit analysis. Therefore dilatancy is related to two competing mechanisms, one that enhances failure due to sliding at the joints, when dilatancy is low, and another that enhances brick failure when dilatancy is high. These competing effects give the possibility to design mortars providing optimal dilatancy for a given structural system. Differently, cohesion and tensile strength of the masonry joints are found to have negligible influence on the maxi-

Table 11: Maximum deflection observed in the masonry vault at varying of φ^h and ψ^b (φ^b = 35°, ψ^h = 0°, and $f_t = c$ = 0 MPa). Comparison between the numerical results obtained with infinitely rigid blocks and deformable ones.

sliding behaviour	$\varphi^b = \varphi^h$ (°)	$\psi^b = \psi^h$ (°)	Maximum deflection deformable blocks (mm)	rigid blocks (mm)	rigid to def. blocks error (%)
associative	35	35	55.80	57.29	2.67
non-associative	35	0	65.04	84.43	29.8

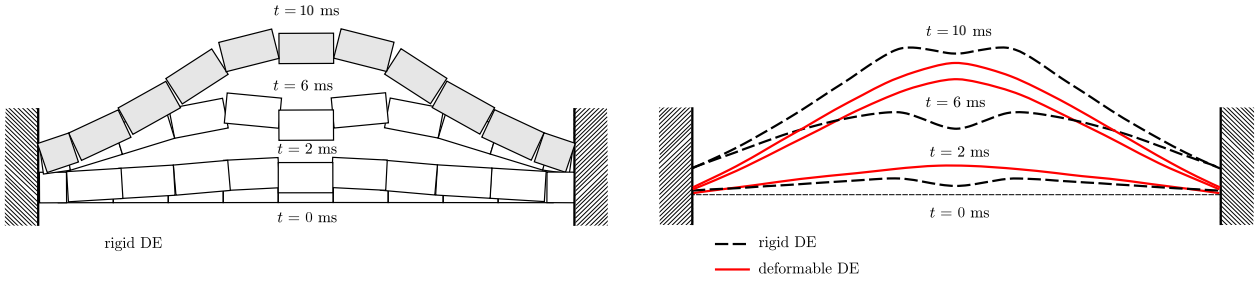

Figure 26: Representative scheme of the rotational locking displayed by infinitely rigid blocks (left) and comparison of the resulting deformed shaped with a deformable blocks model (right), for the non-associative case.

mum deflection, at least for the typical values tested herein ($0 \div 1.5$ MPa for tensile strength and $0 \div 3$ MPa for cohesion).
As far it concerns the effect of the size of the blocks, it was found that in general the larger the blocks are, the higher the strength of the masonry becomes, see also [33, 15, 37].

The numerical simulations showed that the high loading rate effects on the material strength are almost negligible for the structure under study. Indeed, in all of the computations, strain rates were found to be lower than 2 s^{-1}, hence the beneficial effects of high loading rates on the strength of the materials are limited. Moreover, the above mentioned negligible influence of cohesion and tensile strength on the dynamic response of the masonry vault shows that taking into account the high rates phenomena at the material level is unimportant for the investigated system.

It is worth emphasizing that, despite the very good agreement with the experimental results for the planar case, the fineness of the predictions for the curved structure has high computational cost. A common strategy in DEM analyses for reducing this cost is to consider rigid blocks instead of deformable ones. However, such an assumption may affect the predicted structural response when a certain degree of confinement and out-of-plane deformations take place, which is also our case. This is why the assumption of infinitely rigid blocks was also investigated by comparing the numerical results obtained using deformable blocks. For the applications and geometry herein considered, the rigid blocks model underperformed compared to the deformable one. The inferior performance of the rigid blocks is due to the particular cases herein studied which involved out-of-plane loading of confined, shell-like structures. In particular, the rigid block model showed very high stiffness in bending, affecting the deformation modes and therefore the static and dynamic response of the system for both associative and non-associative frictional interfaces. This artificial high bending stiffness was defined here as rotational locking as it is the result of the relative rotations of the building blocks.

The results obtained in this paper can be useful for improving our understanding on the dynamic behaviour of masonry structures under blast actions, for which the scientific literature is limited. Moreover, it gives useful insight and can be used with validation purposes to select appropriate numerical methods based on continuum mechanics (upscaling/homogenization) in the investigation of large masonry structures of non-standard geometry (for which the DEM is prohibitive due to the high computational cost).

References

[1] Abou-Zeid, B. M., El-Dakhakhni, W. W., Razaqpur, A. G., Foo, S., 2011. Response of Arching Unreinforced Concrete Masonry Walls to Blast Loading. Journal of Structural Engineering 137 (10), 1205–1214.

[2] Çaktı, E., Özden Saygılı, Lemos, J. V., Oliveira, C. S., 2016. Discrete element modeling of a scaled masonry structure and its validation. Engineering Structures 126, 224 – 236.

[3] Browning, R. S., Sherburn, J. A., Schwer, L. E., 2013. Predicting blast loads using ls-dyna and cth. In: Proceedings of 2013 ASCE Structures Congress, Pittsburgh.

[4] Bui, T., Limam, A., 2012. Masonry walls under membrane or bending loading cases : experiments and Discrete Element analysis. Proceedings of the 11th International Conference on

Table 12: Maximum deflection observed in the masonry vault at varying of the building blocks size. Comparison between deformable and rigid blocks models, and corresponding relative error, between parentheses. The results are for $c = f_t = 0$ MPa.

sliding behaviour	blocks	$\varphi^b = \varphi^h$ (°)	$\psi^b = \psi^h$ (°)	Maximum deflection 1/2 bocks size (mm)	reference blocks size (mm)	2 blocks size (mm)
associative	deformable	35	35	64.55	55.80	52.08
	rigid			72.25	57.29	69.82
				(11.93 %)	(2.67 %)	(34.06 %)
non-associative	deformable	35	0	70.95	65.04	59.29
	rigid			89.52	84.43	98.98
				(26.17 %)	(29.80 %)	(66.94 %)

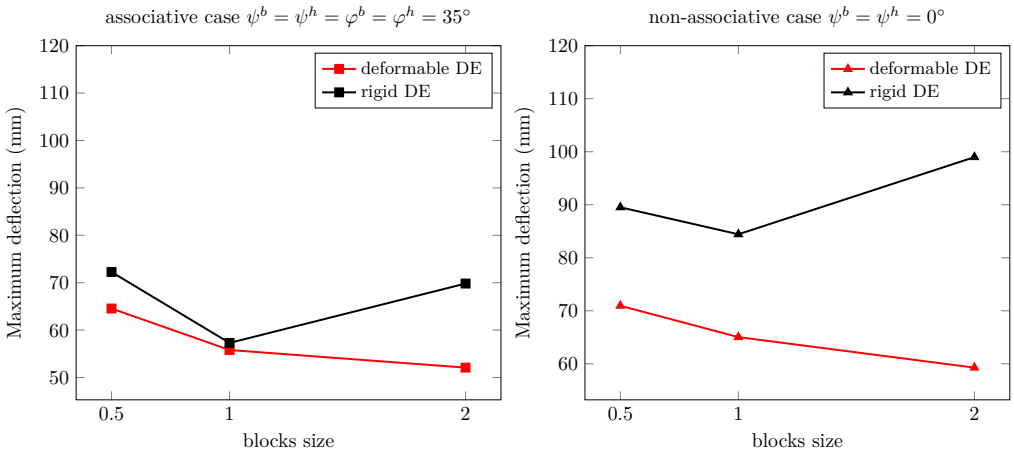

Figure 27: Comparison of the response of the masonry vault in terms of deflection in the proximity of fixed supports (left) and at the centre of the vault's key (right) for different size of the building blocks. The results are for $\varphi^h = 10°$, $\psi^b = 0°$, and $c = f_t = 0$ MPa.

Computational Structures Technology, Dubrovnik, Croatia, 4–7 September.

[5] Bui, T.-T., Limam, A., Sarhosis, V., 2019. Failure analysis of masonry wall panels subjected to in-plane and out-of-plane loading using the discrete element method. European Journal of Environmental and Civil Engineering.

[6] Cascini, L., Gagliardo, R., Portioli, F., 2018. LiABlock_3D: A Software Tool for Collapse Mechanism Analysis of Historic Masonry Structures. International Journal of Architectural Heritage, 1–20.

[7] Chen, X., Wu, S., Zhou, J., 2014. Experimental Study on Dynamic Tensile Strength of Cement Mortar Using Split Hopkinson Pressure Bar Technique. Journal of Materials in Civil Engineering 26 (6), 04014005.

[8] Dennis, S. T., Baylot, J. T., Woodson, S. C., 2002. Response of 1/4-Scale Concrete Masonry Unit (CMU) Walls to Blast. Journal of Engineering Mechanics 128 (2), 134–142.

[9] Douthe, C., Mesnil, R., Orts, H., Baverel, O., 2017. Isoradial meshes: Covering elastic gridshells with planar facets. Automation in Construction 83, 222–236.

[10] Forgács, T., Sarhosis, V., Bagi, K., 2017. Minimum thickness of semi-circular skewed masonry arches. Engineering Structures 140, 317 – 336.

[11] Freund, L., 1972. Crack propagation in an elastic solid subjected to general loading—i. constant rate of extension. Journal of the Mechanics and Physics of Solids 20 (3), 129 – 140.

[12] Freund, L., 1972. Crack propagation in an elastic solid subjected to general loading—ii. non-uniform rate of extension. Journal of the Mechanics and Physics of Solids 20 (3), 141 – 152.

[13] Gabrielsen, B., Wilton, C., Kaplan, K., 1975. Response of arching walls and debris from interior walls caused by blast loading. Tech. rep., URS Reasearch Company, San Mateo. CA.

[14] Gagnet, E. M., Hoemann, J. M., Davidson, J. S., 2017. Assessment of resistance definitions used for blast analysis of unreinforced masonry walls. International Journal of Protective Structures 8 (1), 125–151.

[15] Godio, M., Stefanou, I., Sab, K., May 2018. Effects of the dilatancy of joints and of the size of the building blocks on the mechanical behavior of masonry structures. Meccanica 53 (7), 1629–1643.

[16] Godio, M., Stefanou, I., Sab, K., Sulem, J., Sakji, S., 2017. A limit analysis approach based on cosserat continuum for the evaluation of the in-plane strength of discrete media: Application to masonry. European Journal of Mechanics - A/Solids 66, 168 – 192.

[17] Hyde, D., 1991. ConWep: Conventional weapons effects program. US Army Engineer Waterways Experiment Station, USA.

[18] Itasca Consulting Group, Inc., 2013. 3DEC 5.0 . Minneapolis, MN 55401.

[19] Karlos, V., Solomos, G., Larcher, M., 2016. Analysis of blast parameters in the near-field for spherical free-air explosions. Tech. rep., Joint Research Center of the European Commission.

[20] Keys, R. A., Clubley, S. K., 2017. Experimental analysis of debris distribution of masonry panels subjected to long duration blast loading. Engineering Structures 130, 229 – 241.

[21] Kingery, C. N., Bulmash, G., 1984. Technical report ARBRL-TR-02555: Air blast parameters from TNT spherical air burst and hemispherical burst. Tech. rep., U.S. Army Ballistic Research Laboratory.

[22] Larcher, M., Casadei, F., 2010. Explosions in Complex Geome-

tries — A Comparison of Several Approaches. International Journal of Protective Structures 1 (2), 169–195.
[23] Lemos, J., 2007. Numerical issues in the representation of masonry structural dynamics with Discrete Elements. Proceedings of the 1st ECCOMAS Thematic Conference on Computational Methods in Structural Dynamics and Earthquake Engineering (COMPDYN 2019), Papadrakakis, Fraiadakis (eds), Crete, Greece, 13–15 June, 1126.
[24] Lemos, J., 2017. Contact representation in rigid block models of masonry. International Journal of Masonry Research and Innovation 2, 321–334.
[25] Lemos, J., 2019. Discrete Element Modeling of the Seismic Behavior of Masonry Construction. Buildings 9 (43).
[26] Li, Z., Chen, L., Fang, Q., Hao, H., Zhang, Y., Xiang, H., Chen, W., Yang, S., Bao, Q., 2017. Experimental and numerical study of unreinforced clay brick masonry walls subjected to vented gas explosions. International Journal of Impact Engineering 104, 107 – 126.
[27] Lourenço, P. B., PhD Thesis, 1997. Computational strategies for masonry structures. TU Delft, The Netherlands.
[28] Lourenço, P. B., Ramos, L. F., 2004. Characterization of cyclic behavior of dry masonry joints. Journal of Structural Engineering 130 (5), 779–786.
[29] Luís C. Silva and Paulo B. Lourenço and Gabriele Milani, 2017. Rigid block and spring homogenized model (HRBSM) for masonry subjected to impact and blast loading. International Journal of Impact Engineering 109, 14 – 28.
[30] Macorini, L., Izzuddin, B. A., 2014. Nonlinear Analysis of Unreinforced Masonry Walls under Blast Loading Using Mesoscale Partitioned Modeling. Journal of Structural Engineering 140 (8), A4014002.
[31] Malomo, D., DeJong, M. J., Penna, A., 2019. Distinct element modelling of the in-plane cyclic response of urm walls subjected to shear-compression. Earthquake Engineering & Structural Dynamics.
[32] Masi, F., Stefanou, I., Vannucci, P., Maffi-Berthier, V., 2019. A discrete element method approach for the preservation of the architectural heritage against explosions. Proceedings of the 12th International Congress on Mechanics Thessaloniki (HSTAM), Thessaloniki, Greece, 22-25 September.
[33] Masi, F., Stefanou, I., Vannucci, P., Maffi-Berthier, V., 2019. Rocking response of inverted pendulum structures under blast loading. International Journal of Mechanical Sciences 157-158, 833 – 848.
[34] Michaloudis, G., Gebbeken, N., 2019. Modeling masonry walls under far-field and contact detonations. International Journal of Impact Engineering 123, 84 – 97.
[35] Parisi, F., Balestrieri, C., Asprone, D., 2016. Blast resistance of tuff stone masonry walls. Engineering Structures 113, 233 – 244.
[36] Petry, S., 2015. Force-displacement response of unreinforced masonry walls for seismic design. Tech. rep., École Polytechnique Fédérale de Lausanne, EPFL.
[37] Petry, S., Beyer, K., Dec 2014. Scaling unreinforced masonry for reduced-scale seismic testing. Bulletin of Earthquake Engineering 12 (6), 2557–2581.
[38] Petry, S., Beyer, K., 2015. Cyclic test data of six unreinforced masonry walls with different boundary conditions. Earthquake Spectra 31 (4), 2459–2484.
[39] Rafsanjani, S. H., Lourenço, P., Peixinho, N., 2015. Implementation and validation of a strain rate dependent anisotropic continuum model for masonry. International Journal of Mechanical Sciences 104, 24 – 43.
[40] Remennikov, A. M., 2003. A review of methods for predicting bomb blast effects on buildings. Journal of Battlefield Technology 6, 5–10.
[41] Ross, C. A., Tedesco, J. W., Kuennen, S. T., 1995. Effects of strain rate on concrete strength. Materials Journal 92 (1), 37–47.
[42] Sarhosis, V., Bagi, K., Lemos, J. V., Milani, G., 2016. Computational modeling of masonry structures using the discrete element method. IGI Global.
[43] Shin, J., Whittaker, A. S., Cormie, D., 2015. Incident and normally reflected overpressure and impulse for detonations of spherical high explosives in free air. Journal of Structural Engineering 141 (12), 04015057–13.
[44] Stefanou, I., Psycharis, I., Georgopoulos, I.-O., 2011. Dynamic response of reinforced masonry columns in classical monuments. Construction and Building Materials 25 (12), 4325 – 4337.
[45] Stefanou, I., Sab, K., Heck, J.-V., 2015. Three dimensional homogenization of masonry structures with building blocks of finite strength: A closed form strength domain. International Journal of Solids and Structures 54, 258–270.
[46] Stefanou, I., Sab, K., Heck, J.-V., 2015. Three dimensional homogenization of masonry structures with building blocks of finite strength: A closed form strength domain. International Journal of Solids and Structures 54, 258 – 270.
[47] van der Pluijm, R., 1999. Out-of-Plane bending of Masonry. Behavior and Strength. Technische Universiteit Eindhoven.
[48] Vannucci, P., Masi, F., Stefanou, I., 2017. A study on the simulation of blast actions on a monumental structure.
URL https://hal.archives-ouvertes.fr/hal-01447783v3/document
[49] Vannucci, P., Masi, F., Stefanou, I., 2019. A nonlinear approach to the wind strength of Gothic Cathedrals: The case of Notre Dame of Paris. Engineering Structures 183, 860 – 873.
[50] Vannucci, P., Masi, F., Stefanou, I., Maffi-Berthier, V., 2019. Structural integrity of Notre Dame Cathedral after the fire of April 15th, 2019.
URL https://hal.archives-ouvertes.fr/hal-02105786v2
[51] Vannucci, P., Stefanou, I., Masi, F., 2017. Cathédrales Durables. Tech. rep., CNRS, Paris.
[52] Varma, R. K., Tomar, C. P. S., Parkash, S., Sethi, V. S., 1997. Damage to brick masonry panel walls under high explosive detonations. Pressure vessels and piping division. ASME 351, 207 – 216.
[53] Vélez, L. F. R., Magenes, G., Griffith, M. C., 2014. Dry stone masonry walls in bending—part i: Static tests. International Journal of Architectural Heritage 8 (1), 1–28.
[54] Wang, M., Hao, H., Ding, Y., Li, Z.-X., 2009. Prediction of fragment size and ejection distance of masonry wall under blast load using homogenized masonry material properties. International Journal of Impact Engineering 36 (6), 808 – 820.
[55] Weerheijm, J., 1992. Concrete under impact tensile loading and lateral compression. Ph.D. thesis, TU Delft, Delft University of Technology.
[56] Wei, X., Stewart, M. G., 2010. Model validation and parametric study on the blast response of unreinforced brick masonry walls. International Journal of Impact Engineering 37 (11), 1150 – 1159.
[57] Whiting, E., Shin, H., Wang, R., Ochsendorf, J., Durand, F., 2012. Structural optimization of 3D masonry buildings. ACM Transactions on Graphics (TOG) 31 (6), 159.
[58] Wild, S., Gailius, A., Hansen, H., Pederson, L., Szwabowski, J., 1997. Pozzolanic properties of a variety of European clay bricks. Building Research & Information 25 (3), 170–175.